

Using a Knowledge-Based Approach to Remove Blocking Artifacts in Skin Images for Forensic Analysis

*Chaoying Tang, *IEEE Student Member*, Adams Wai-Kin Kong, *IEEE Member*, and Noah Craft

Abstract — Identifying individuals in evidence images, where their faces are covered or obstructed, is a challenging task. In the legal case, *United States v. Michael Joseph Pepe (2008)*, Craft and Kong, who served as expert witnesses, used pigmented skin marks to identify a suspect in evidence images. Their expert opinions were challenged, partially because the blocking artifacts generated by the standard JPEG algorithm adversely affect the visibility of the small skin marks. In addition to this case, a huge amount of JPEG compressed child pornography is posted on-line every day. Although many methods have been developed to remove blocking artifacts, they are ineffective for our target application. In this paper, a knowledge-based (KB) approach, which simultaneously removes JPEG blocking artifacts, and recovers skin features, is proposed. Given a training set containing both original and compressed skin images, the relationship between original blocks and compressed blocks can be established. This prior information is used to infer the original blocks of compressed evidence images. A Markov-model-based algorithm and a faster one-pass algorithm were developed to make inference, and a block synthesis algorithm was developed to handle the cases where compressed blocks are not contained in the training set. An indexing mechanism was also proposed to deal with large datasets efficiently. Extensive experiments were conducted on images with different characteristics and compression ratios. Both subjective and objective evaluations demonstrated that the KB approach is more effective than other methods. In summary, the KB approach is capable of removing blocking artifacts to recover useful skin features.

Index Terms – Markov model, pornography, vein pattern, skin mark, biometrics

Copyright (c) 2010 IEEE. Personal use of this material is permitted. However, permission to use this material for any other purposes must be obtained from the IEEE by sending a request to pubs-permissions@ieee.org.

Chaoying Tang and Adams Wai-Kin Kong are with the Forensics and Security Laboratory, School of Computer Engineering, Nanyang Technological University. E-mail: tangchaoying@pmail.ntu.edu.sg, adamskong@ntu.edu.sg.

Noah Craft is with Los Angeles Biomedical Research Institute at Harbor-UCLA Medical Center. E-mail: ncraft@ucla.edu.

1. Introduction

Recent technological advances have led to a proliferation of digital media. This media is commonly used during investigations and as evidence in legal cases. Improving the capacity and quality of processing this media for criminal and victim identification is becoming an important task. In some cases (e.g. child pornography and masked gunmen), faces of criminals cannot be seen because they are covered or obstructed. Biometric traits in skin (e.g. skin marks and veins) could be important features for personal identification. Two authors (N.C. and A.K.) were recruited by the U.S. Department of Justice as expert witnesses for a legal case, *United States v. Michael Joseph Pepe (2008)*, which involved sexual acts with seven pre-teen girls in Cambodia [1]. N.C. (a board-certified dermatologist) identified pigmented and vascular skin marks in digital images (evidence images) collected from a crime scene. Because the face of the criminal in the evidence images could not be observed, N.C. also identified similar skin marks on a suspect in custody for personal verification. Although prosecuted under the “Prosecutorial Remedies and Other Tools to end the Exploitation of Children Today” or PROTECT Act of 2003, the suspect was returned to the U.S., convicted, and was sentenced to 210 years in prison. During the legal proceedings, the defense attorneys raised several issues including the fact that digital blocking artifacts could adversely influence the visibility of skin marks in the evidence.

In addition to this case, a significant amount of child pornography has been posted on the Internet. In Canada alone, 30,000 cases of child pornography have been reported [2]. The U.S. Customs Service estimated that 100,000 websites offer child pornography [3]. The Bureau of Justice Statistics reported that child sex offenses are the fastest growing offenses of the Federal criminal caseload, and child pornography made up 69% of child sex offenses [4]. The exact statistics concerning the percentage of JPEGs in pornography is unavailable. However, because the JPEG algorithm is an international standard and has been widely installed in digital cameras, we believe most of the still images used for child pornography are compressed by the JPEG algorithm.

Using biometric traits from the skin for criminal and victim identification highly depends on the quality of evidence images, because the size of these traits in the images is usually very small. Digital

images, taken by consumer cameras, are always compressed by the JPEG algorithm. Blocking artifact is a well-known problem caused by this algorithm. As a result, vein patterns can be broken, and skin marks can be blurred, or even totally removed, especially under high compression ratios. Fig. 1 illustrates the effects of blocking artifacts on pigmented skin marks and vein patterns. Thus, technology to remove blocking artifacts could improve images before any forensic analyses.

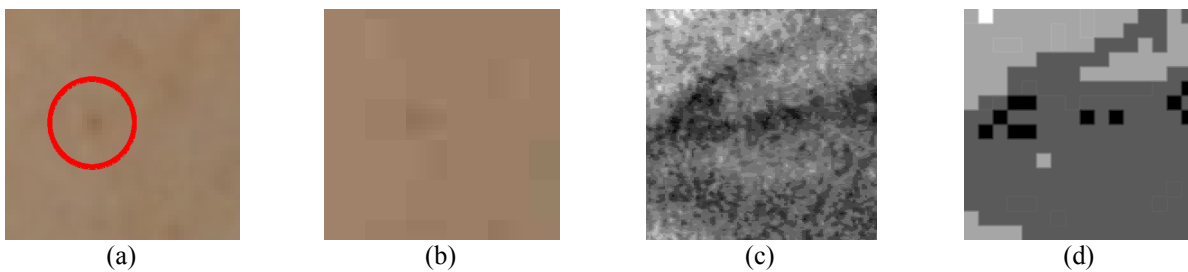


Fig. 1 Illustration of the effects of blocking artifacts on pigmented skin marks and veins. (a) Uncompressed color image with a common nevus and (c) ¹V component with a clear vein pattern. (b) is the JPEG compressed image of (a) with compression ratio of 102.51 and quality factor of 25. (d) is the JPEG compressed image of (c) with compression ratio of 95.63 and quality factor of 25.

There is a considerable amount of research on approaches to remove JPEG blocking artifacts. These approaches can be classified into two categories [5]. The first category addresses the problem at the encoder side. These are known as pre-processing methods. These can be further sub-classified into two groups: “pre-filtering” [6]-[7], which removes unnoticeable details in source images so that less information has to be coded, and special “encoding/transformation”, such as perceptual-based coding [8] and poly-harmonic local cosine transformation [9]. These methods are impractical for use in forensic applications, because they require modifications to the encoder (camera). However, during forensic analysis of digital images, the photographs involved in the crimes have already been compressed.

The second category uses post-processing techniques at the decoder side. Generally speaking, they can also be sub-classified into two groups: image enhancement and image restoration. The goal of the image enhancement algorithms is to improve the perceived quality subjectively. They take into account the special structure of blocking artifacts and human visual sensitivities. The most popular and straightforward enhancement method is to apply low-pass filters to the region where artifacts occur. Filtering can be

¹ The JPEG algorithm transforms an image from RGB space to YUV space before performing the DCT Transform.

performed either in the spatial domain [10]-[11] or in the frequency domain [12]-[13]. Other filtering methods integrate neural networks or fuzzy schemes [14]-[15]. For these methods, adaptivity is necessary to avoid image blurring. However, the adaptation to local statistics relies on a good classification scheme, which is usually sensitive to quantization and compression ratio. Poor estimation and adaptation can sometimes cause image quality degradation. Another enhancement approach is to recover quantized AC coefficients from DC coefficients of a given block and its neighboring blocks [16]. This method can considerably reduce the blocking artifacts in smooth areas, but the prediction is not reliable in the neighborhood of edges.

Post-processing through image restoration aims to recover the lost information based on prior knowledge. A number of classical image restoration algorithms have been tailored for deblocking artifacts. They can be further sub-classified into two approaches: criterion-based methods and constraint-based methods. The basic concept of the criterion-based methods is to find an optimal image from a JPEG compressed image based on some predefined criteria. For generic images, the best criterion is usually perceptual image quality. However, modeling perceptual image quality is still an on-going research topic. The minimum mean square error (MSE) [17] and maximum a posteriori (MAP) probability [23] are the commonly used criteria. The major drawback with MSE-based methods is that MSE is not very well matched to perceptual visual quality [27]. For the MAP-based methods, previous models were designed for generic images, and therefore, prior knowledge from new target images cannot be used to recover the lost information.

The basic idea behind the constraint-based methods is to impose constraints on compressed images and to restore them accordingly. The projection onto convex sets (POCS) method is a typical example. The constraint sets are defined as closed convex sets, whose elements are consistent with prior knowledge of original images. A feasible solution in the intersection of all the sets can be found via an iterative process [18]-[19]. POCS-based methods have two limitations. Firstly, users are required to define the projection operation for every constraint set [20]. Improper operations may lead to divergence and ultimately provide

results even worse than compressed images. Secondly, their computational complexity is extremely high, because they perform both forward and inverse DCT calculations during each cycle of an iterative process.

All the current deblocking methods were designed for generic images, and therefore, cannot utilize prior knowledge from target images. In fact, these methods make the situation even worse, because they generally smooth images, including biometric traits, to alleviate blocking artifacts. Fig. 2 shows resultant images from some of these methods. In addition, the difference between original (uncompressed) images and their resultant images may be even larger than that between original images and compressed images in terms of quantized Discrete Cosine Transform (QDCT) coefficients.

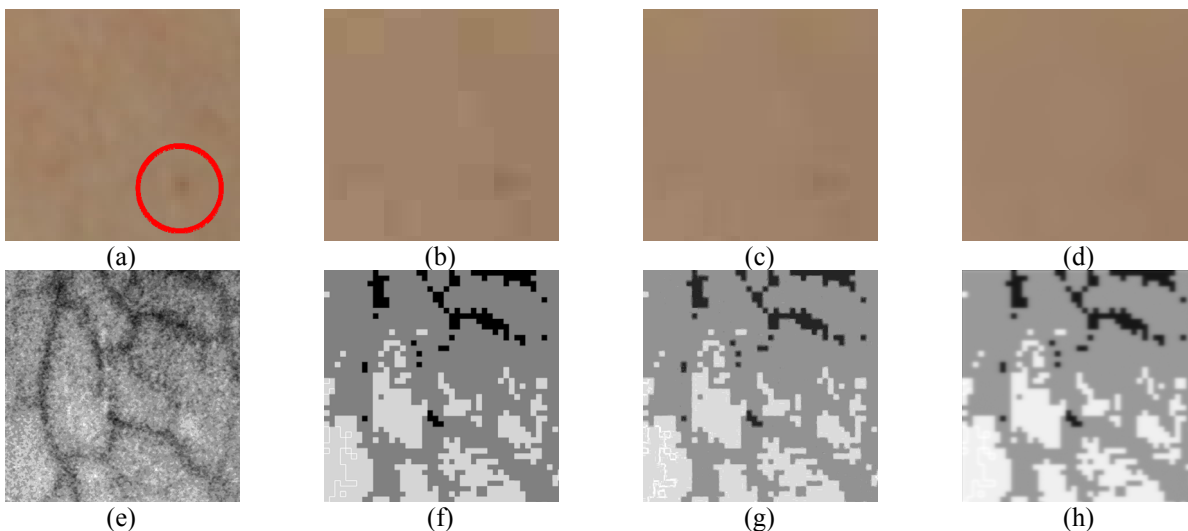


Fig. 2 Illustration of the smoothing effect of traditional deblocking methods on skin images. (a) Uncompressed color image with a common nevus and (e) V component with a clear vein pattern. (b) is the JPEG compressed image of (a) with compression ratio of 115.32 and quality factor of 25. (f) is the JPEG compressed image of (e) with compression ratio of 120.15 and quality factor of 25. (c) and (g) are respectively the results of (b) and (f) from a post-filtering method [25]. (d) and (h) are respectively the results of (b) and (f) from a MAP-based method [23].

To overcome the deblocking issues outlined above, we developed a new approach to remove blocking artifacts in skin images. We use a non-parametric approach to extract prior knowledge, i.e., the block relationship between compressed blocks and their original counterparts, and the neighborhood relationship among adjacent original blocks. We then developed two different algorithms to make inferences based on this prior knowledge. The first one uses a Markov model and the belief propagation algorithm. This algorithm may be more accurate but requires more time. The second one is faster and is a one-pass

algorithm utilizing spatial and frequency relationships simultaneously. Both algorithms require that at least one compressed block in a training set shares the same QDCT with the input compressed block. To remove this requirement, a block synthesis algorithm is proposed.

The rest of this paper is organized as follows. Section 2 introduces the prior knowledge in skin images. Section 3 presents our knowledge-based (KB) approach including the Markov-model-based, the one-pass and the block synthesis algorithms. We also present an indexing mechanism to improve the speed of the algorithms. Section 4 reports objective and subjective experimental results. Section 5 offers some concluding remarks.

2. Prior Knowledge in Skin Images

To exploit prior knowledge in skin images, we constructed a large database composed of skin images collected from different body sites, including the hand, arm, foot, leg, chest and back. We divided the database into a training set and two testing sets. We extracted prior information from the training set to develop the KB approach and then used the testing sets to evaluate its function.

2.1. Database

Our database consists of two parts. The first part (Asian database) was collected in Singapore from 97 Asians with both genders and diverse ages, occupations, and body mass indices (BMI). The ethnic groups include Chinese, Malay, Indian, and Javanese. They are between 12 and 70 years old. Their occupations include students, professors, and manual workers, and their BMIs range from 18 to 40. The camera model was Nikon D70s, and the images were taken under normal daylight or fluorescent light. The second part (Caucasian database) was collected in the United States from 10 Caucasians under Institutional Review Board approval from the Los Angeles Biomedical Research Institute. The camera model was Nikon D80, and the imaging configuration such as illumination and image distance was also different from the settings in Singapore. We used images from 71 randomly selected subjects in the Asian database to form a training set. Five of them are females. Their races include Chinese, Malay, Indian and Javanese. Their ages range

from 18 to 59, and BMIs range from 19 to 27. The images were taken from different body parts, including the hand, arm, thigh, leg, chest and back (see Fig. 3). We only used images in the Asian database to form the training set in order to demonstrate that the proposed KB approach can work well, even when input images and training images have very different characteristics (e.g. different imaging conditions and races). This experimental design is more appropriate because in legal cases, we cannot guarantee evidence images and training images will have the same characteristics. The remaining 26 subjects' images in the Asian database comprised the first testing set. The images in the Caucasian database comprised the second testing set. Each set has participants from both genders and all age groups. These images were stored in the JPEG format with a very high quality factor of 99 and without noticeable blocking artifacts. The original images from the cameras are referred to as uncompressed images.

For the training set, because a large part of the raw images is background, we cropped sub-images with 256×256 pixels containing only areas of visible skin. This relatively small size was chosen to reduce redundant information and improve the speed of the algorithms. Then we used the JPEG algorithm to compress the sub-images resulting in image pairs. Each pair has one original skin image and the corresponding JPEG compressed image. After cropping, the training set contained 5,662 image pairs. Fig. 4 illustrates a raw image (4a) and a pair of skin sub-images obtained from it (4b and 4f). The KB approach is operated in the YUV space because the JPEG compression is performed in this space. Fig. 4(h) and Fig. 4(i) show that the blocking artifacts in the U and V components are more significant. These artifacts are caused primarily because of the down-sampling process in the JPEG algorithm and because of larger quantization steps. By further cutting the image pairs into 8×8 pixel blocks, we have 5,797,888 block pairs in the training set. By choosing different compression quality factors we then obtained different training sets.

For the first testing set, we cropped 500 skin sub-images with size of 448×512 or 512×448 pixels from the raw images of the 26 Asian subjects. We chose the larger sizes in order to cover more skin features. For the second testing set, we cropped 262 skin sub-images with size of 256×256 pixels from the raw images of the 10 Caucasians. Because Caucasians have more pigmented skin marks, we used the

second testing set to evaluate the performance of the KB approach on skin marks. We chose the smaller size so that skin marks can be easily observed.

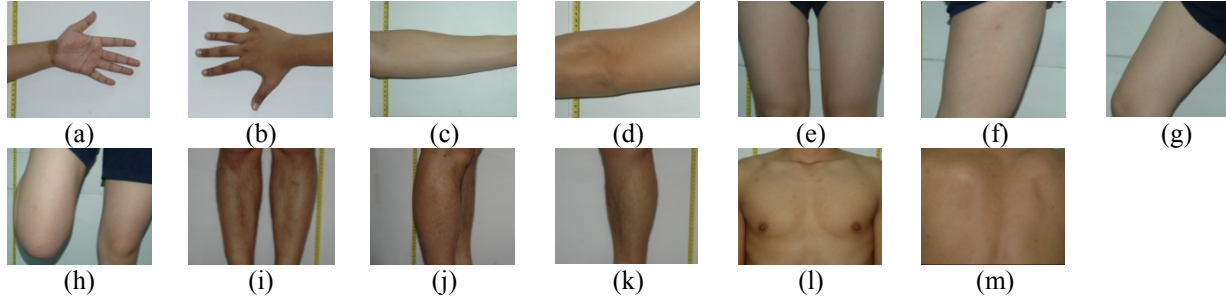


Fig. 3 Illustration of some images in the training set. (a)-(b) hands of a female (Indian, 20 years old), (c)-(d) arms of a male (Chinese, 23 years old), (e)-(h) thighs of a female (Chinese, 21 years old), (i)-(k) legs of a male (Chinese, 33 years old), (l) chest, and (m) back of a male (Chinese, 23 years old).

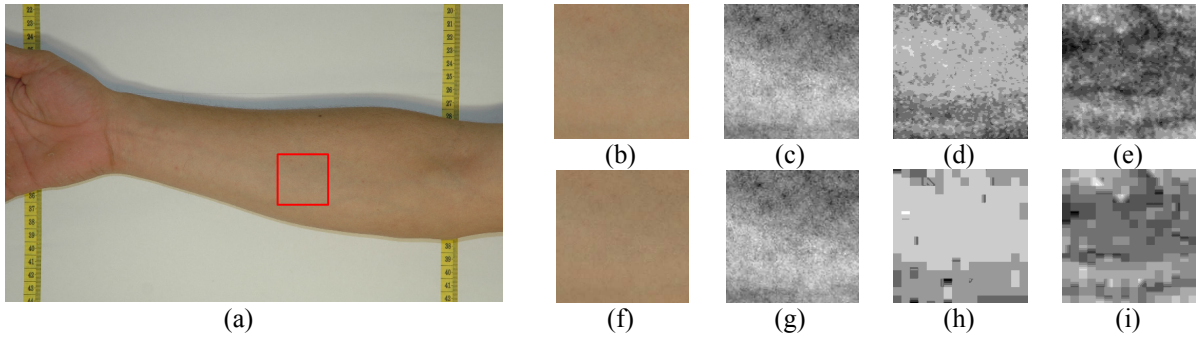


Fig. 4 Illustration of a raw image and a pair of skin images obtained from it. (a) A raw image of the inner right forearm of a male (Chinese, 52 years old, BMI = 25). (b) The skin image cropped from the red rectangle in (a). (c), (d) and (e) are the Y, U and V components of (b). (f) is the JPEG compressed image of (b) with the compression ratio of 41.98 and quality factor of 50. (g), (h) and (i) are the Y, U and V components of (f).

2.2. Training Blocks

The relationship between an original block and its compressed result is that they have the same QDCT coefficients. In general, only several coefficients in the upper left corner of a QDCT matrix are non-zero integers. We call them effective coefficients, and use them to form an index vector. Fig. 5 illustrates a QDCT coefficient matrix, the effective coefficients, and the corresponding index vector. Because the quantization is a many-to-one mapping, different original blocks can have the same QDCT coefficients and index vector. Fig. 6(a) shows a compressed block in the V component. Figs. 6(b)-(k) are some original blocks which can be compressed to Fig. 6(a). All their index vectors are $[13 \ 0 \ 0 \ 0 \ 0 \ 0 \ 0 \ 0 \ 0]$, where only the DC term is non-zero and therefore, Fig. 6(a) has only one intensity value. This many-to-one block

relationship implies that only the local information inside one block is not sufficient to uniquely determine corresponding original blocks. We also considered the relationship between neighboring blocks. For each original block, we defined two neighborhoods: a frequency neighborhood, which is composed by the index vectors of the 8 neighboring blocks; and a spatial neighborhood, which is composed by the 36 pixels in the 8 neighboring blocks which are connected with the target block (as illustrated in Fig. 7).

These block and neighborhood relationships represent the prior knowledge in skin images. They are extracted from the training set to infer original blocks in evidence images. We developed two algorithms to make inference, which will be discussed in the following section.

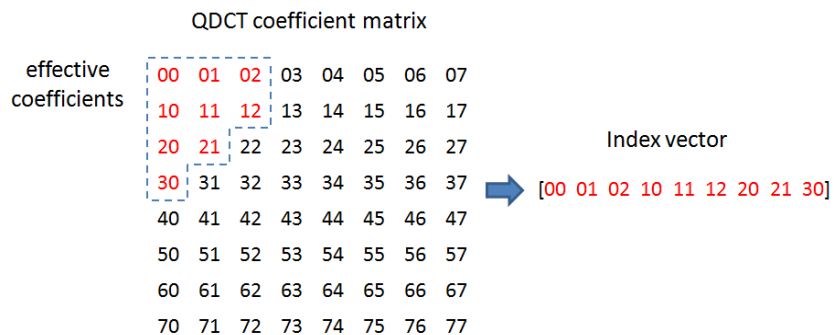


Fig. 5 Illustration of QDCT coefficient matrix, effective coefficients, and index vector.

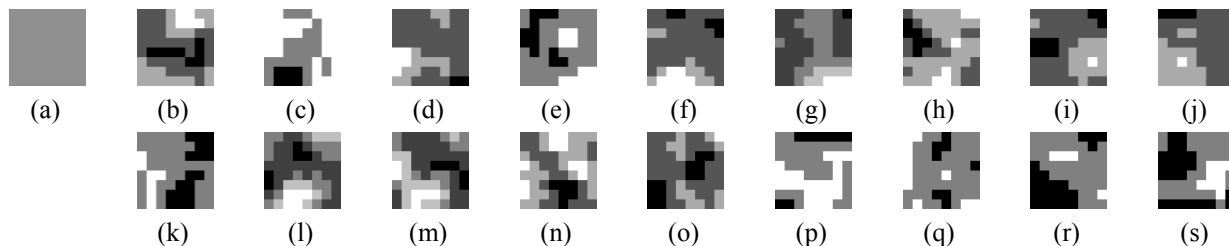


Fig. 6 Illustration of a compressed block and its corresponding original blocks. (a) is a compressed block, (b)-(s) are the corresponding original blocks of (a).

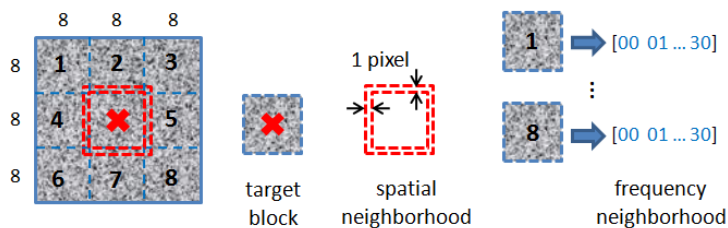


Fig. 7 Illustration of spatial and frequency neighborhoods.

3. The Two Inference Algorithms based on Prior Knowledge

In this section, we present two algorithms to make inference based on prior knowledge: one is based on a Markov model, while the other is a one-pass algorithm. We also present a block synthesis algorithm to handle the cases where the training set does not contain input compressed blocks. To speed up these algorithms, an indexing mechanism was also developed.

3.1. An Algorithm based on a Markov Model

The first algorithm uses the traditional Markov model illustrated in Fig. 8, where the circles represent network nodes, and the lines indicate statistical dependencies between nodes [21]. Let compressed blocks be observation nodes, y , and original blocks with corresponding QDCT coefficients be the different states of hidden nodes, x , which we seek to estimate [22]. For this network, the probability of any choice of original blocks is proportional to the product of functions $\varphi_i(x_i, y_i)$ relating each observation to the underlying hidden states, and compatibility functions $\psi_i(x_i)$ relating the possible states of neighboring hidden nodes i.e.,

$$P(x | y) \propto \prod_{i=1}^M \varphi_i(x_i, y_i) \prod_{i=1}^M \psi_i(x_i), \quad (1)$$

where M is the number of blocks. The function $\varphi_i(x_i, y_i)$ can be specified by the JPEG compression algorithm:

$$\varphi_i(x_i, y_i) = \delta\{Q[DCT(x_i)] - Q[DCT(y_i)]\}, \quad (2)$$

where $DCT(\cdot)$ represents the DCT transform, $Q[\cdot]$ is the quantization operator, and δ is a delta function.

The function $\psi_i(x_i)$ represents the spatial compatibility between neighboring original blocks. Let p_{ij}^s be pixels in the spatial neighborhood (see Fig. 7) of block i which overlap with the neighboring block j ($j \in N(i)$, where $N(i)$ is the 8 neighbors of block i). Let p_{ji} be pixels in the neighboring block j which overlap with the spatial neighborhood of block i . The compatibility function is defined as:

$$\psi_i(x_i) = \exp \left(- \frac{\left[\sum_{j \in N(i)} |p_{ij}^s - p_{ji}| \right]^2}{2\sigma^2} \right). \quad (3)$$

The optimal original blocks are the collection that maximizes the probability of the Markov network. Finding the global optimal solution is computationally intractable, so we used belief propagation to obtain a suboptimal solution. The σ in the Eq. 3 can be removed from the optimization formulation because φ_i can be considered as constraints and all ψ_i s are multiplied together in Eq. 1.

Fig. 9 illustrates the performance of the algorithm based on the Markov model. Fig. 9(a) is the V component of an original skin sub-image where one can observe a patterned distribution of hemoglobin in the veins of the skin. However, in the compressed image, the pattern is destroyed (see Fig. 9(b)). We used belief propagation to infer original blocks. At the beginning (zero iteration), a resultant image consists of the original blocks in the training set which have the same index vectors as the compressed blocks. Spatial smoothness is not considered in this initialization. Because there may be more than 10,000 candidate blocks corresponding to one compressed block, we used frequency neighborhoods (see Fig. 7) as a constraint to reduce the searching range. However, the result was still noisy and had many repeated blocks (see Fig. 9(c)). A high compression ratio of 86.92 produces large areas with the same intensity value (see Fig. 9(b)) leading to this effect. In the following iterations, more than half of these estimated blocks are subsequently corrected by belief propagation based on spatial smoothness constraints. It quickly converges after four to five iterations and significantly improves the quality of the result (see Figs. 9(d)-(h)). The vein pattern in the skin is successfully recovered, and the blocking artifacts are completely removed.

Most of other Markov-model-based deblocking algorithms formulate the problem as a minimization based on the Gibbs distribution, but they do not use the relationship between original and compressed blocks. Consequently, they cannot guarantee that compressed images and their resultant images have the same QDCT coefficients. The proposed KB approach uses the functions φ_i to represent the JPEG

compression constraints, which ensure that deblocked images and corresponding compressed images have the same QDCT coefficients. In addition, it utilizes information from the training database extensively.

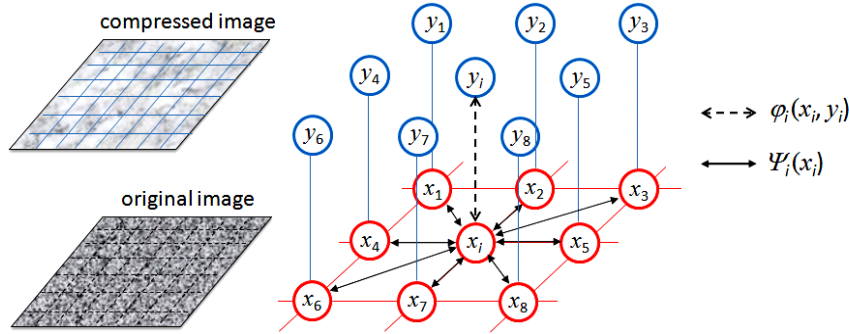


Fig. 8 A Markov network model.

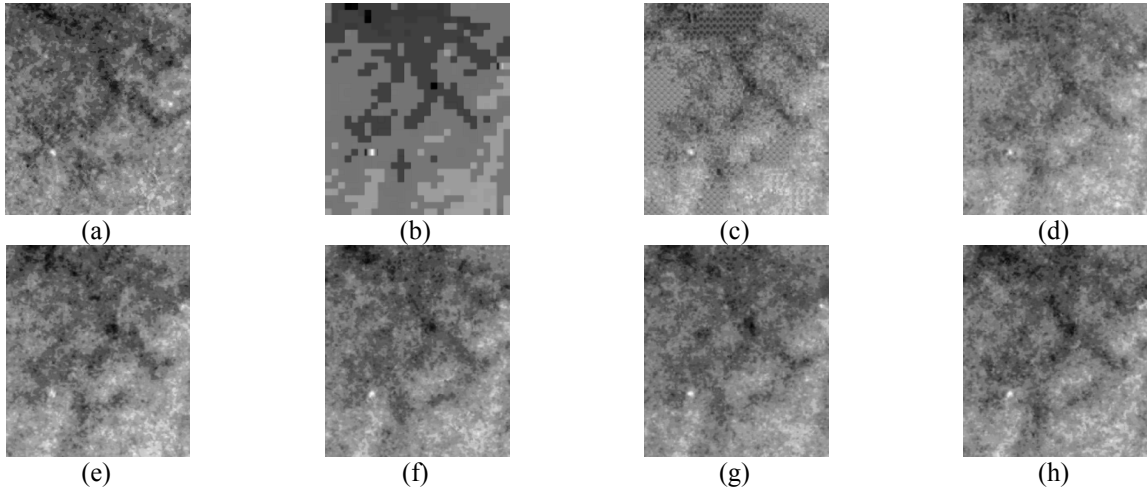


Fig. 9 Illustration of the performance of the Markov-model-based algorithm. (a) The V component of an original skin sub-image. (b) is a compressed version of (a) with the compression ratio of 86.92 and quality factor of 50. (c)-(h) are respectively the results after 0, 1, 3, 6, 9 and 18 iterations.

3.2. A One-Pass Algorithm

Although the belief-propagation algorithm converges quickly, it still needs several iterations to produce a satisfactory result. We also developed a one-pass algorithm that infers original blocks based on combined spatial and frequency information. Assume that a compressed image is processed block by block in a raster-scan order – from left to right and from top to bottom. Thus, for a compressed block target, three upper and one left neighboring blocks have already been processed (illustrated in Fig. 10). The spatial information in the processed blocks (blocks 1-4 in Fig. 10) and the frequency information in the to-be-

processed blocks (blocks 5-8 in Fig. 10) were used as smooth constraints to search the best original block in the training set. The pixels in the processed blocks that are connected to the target block represent the spatial neighborhood. The index vectors of the to-be-processed blocks represent the frequency neighborhood. Together these form the “hybrid neighborhood” of the target block. Thus, each original block in the training set has a hybrid neighborhood determined from the source image (as depicted in Fig. 11). In this way, each record in the training set contains an original block, its hybrid neighborhood, and its compressed block.

In the testing stage, for a target block w , we used its index vector to find a group of candidate original blocks, $G(w) = \{z \mid QDCT[z] = QDCT[w]\}$. Then we searched an optimal candidate according to the hybrid neighborhood of the target block. This search was carried out in two steps. Firstly, we used the frequency neighborhood to narrow down the group i.e.,

$$G'(w) = \{u \in G(w) \mid F_w = F_u\}, \quad (4)$$

where F_w (or F_u) represents the frequency neighborhood of w (or u). If it was an empty set, we searched 20 candidate blocks from $G(w)$ whose frequency neighborhoods are the nearest to F_w to form G' . Then we used the spatial neighborhood to find the optimal original block t^* i.e.,

$$t^* = \arg \min_{t \in G'(w)} d(S_t, S_w), \quad (5)$$

where S_w (or S_t) represents the spatial neighborhood of w (or t), and d represents $L1$ -norm.

To compare the one-pass algorithm with the Markov-model-based algorithm, we used the same testing image (see Fig. 9(b)) to evaluate the one-pass algorithm (see Fig. 12). Theoretically, the result from the Markov-model-based algorithm should be more accurate because it optimizes the probability in Eq. 1. However, Fig. 12(c) and Fig. 12(d) demonstrate that the difference between the two results is difficult to discern with normal human vision. The one-pass algorithm had similar performance but is 12 times faster than belief propagation. Thus, the one-pass algorithm was used for the following evaluations. Fig. 13 illustrates some blocks from Fig. 12. Original blocks in the first row correspond to the compressed blocks in the second row. The high compression ratio causes great information loss. The third and fourth rows are

the resultant blocks from the Markov-model-based and one-pass algorithms, respectively. For the one-pass algorithm, the hybrid neighborhood is sufficient to recover the lost information.

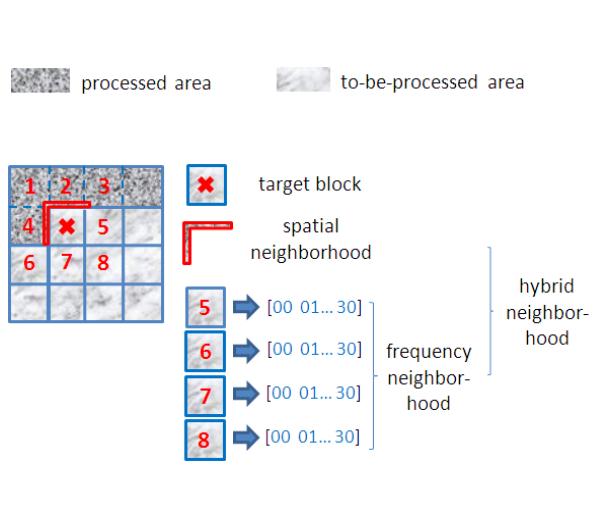


Fig. 10 Illustration of hybrid neighborhood in the testing process.

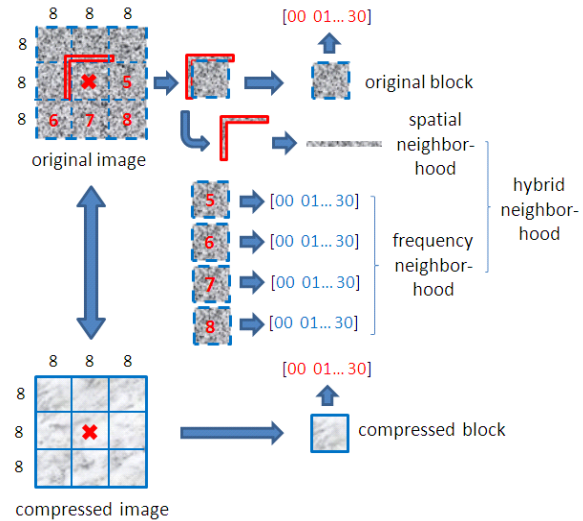


Fig. 11 Illustration of hybrid neighborhood in training set construction.

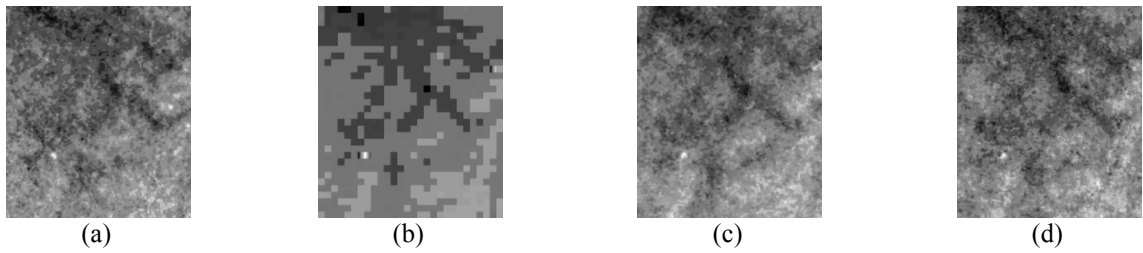


Fig. 12 Illustration of the performance of the one-pass algorithm. (a) The V component of an original skin sub-image. (b) is a compressed version of (a) with the compression ratio of 86.92 and quality factor of 50. (c) is the result from the Markov-model-based algorithm. (d) is the result from the one-pass algorithm.

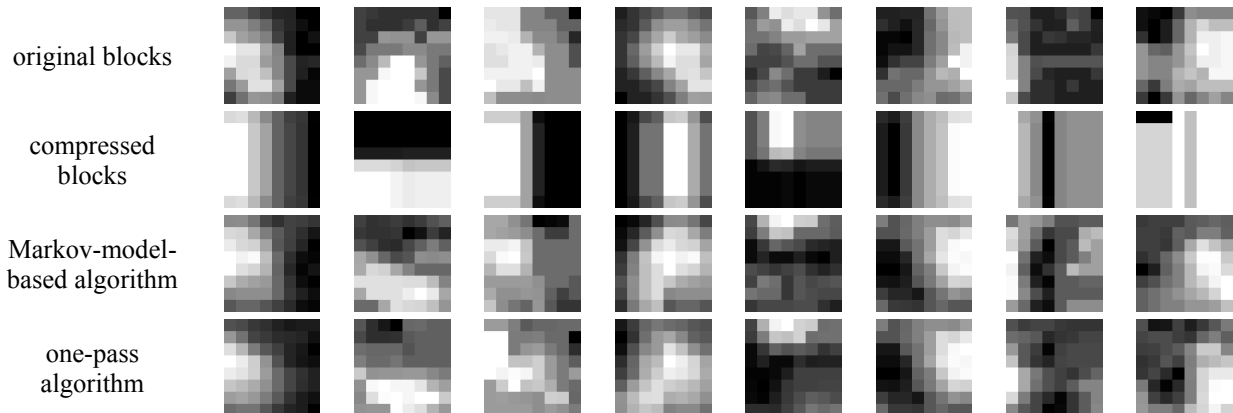


Fig. 13 Illustration of corresponding blocks from Fig. 12. In the first row are the original blocks. In the second row are the corresponding compressed blocks. In the third row are the resultant blocks obtained by the Markov-model-based algorithm. In the fourth row are the resultant blocks obtained by the one-pass algorithm.

3.3. A Block Synthesis Algorithm

Both Markov-model-based and one-pass algorithms require that at least one compressed block in the training set shares the same QDCT coefficients with the input compressed block. The variation of compressed skin blocks and the completeness of our training set are important for the KB approach. In this subsection, we first estimate the variation of compressed skin blocks and present our block synthesis algorithm to remove this requirement.

To estimate the variation of compressed skin blocks and completeness of our training set, we calculated the ranges of QDCT coefficients in our database and assume that all QDCT coefficients are statistically independent. Note that QDCT coefficients are integers. Using the ratios of the estimated total number of different compressed blocks to the total number of compressed blocks in our database as an index, we noted that the variation of compressed blocks is very limited in U and V components, but it is very large in Y component. Under the quality factor of 25, the ratios in U and V components are 0.009% and 0.02%, respectively. Under the quality factor of 50, the ratios in U and V components are 3.21% and 5.11%, respectively. However, for Y component, the ratios under either quality factor are larger than 100%. When the quality factor is higher than 50, the loss of information is not significant, so there is no need for blocking artifact removal.

To handle the cases where input compressed blocks cannot be found in our training set, two or three training blocks were used to synthesize a new block with the same index vector as the input block. Fig. 14 illustrates this block synthesis algorithm. The search of low (high) frequency coefficients was from the rightmost (leftmost) element in the index vector to the left (right) until the quantized coefficients did not match. As a result, the number of overlapping coefficients was maximized to achieve the best compatibility with two blocks. If more than one block had the same number of matched coefficients, we used the hybrid neighborhood as a constraint to select the best one. After that we combined their DCT matrices and took inverse DCT transform to obtain the synthetic block. For the overlapping part, we used the DCT coefficients of the low frequency block. If two source blocks were not sufficient to cover the index vector, the third one would be used for the remaining coefficients. An iterative process was used to

identify this block. In each iteration, the search was performed in three situations: one coefficient was removed from the rightmost part, the leftmost part, and each part. If no candidate was found, the coefficients were continuously removed until one block was found. In our experiment, more than 99.9% of the compressed blocks could be replaced with a source block or a synthetic block from two or three source blocks. With the increase in the database size, we can further reduce the percentage of non-replaced blocks. Note that we used 1D index vector instead of 2D plane to find coefficients because the former is easier to handle and offers higher searching speed. Fig. 15 shows some results of this algorithm. The first row contains original blocks and the second row contains the corresponding compressed blocks. The third row contains the synthetic blocks obtained from the source blocks shown in the fourth and fifth rows. These results demonstrate that our algorithm has the capability to synthesize new blocks whose compressed blocks are not in the training set. Therefore, the KB approach can recover skin patterns “unknown” to the database. The synthetic blocks in Fig. 15 are more similar to their high frequency blocks than their low frequency blocks because (1) human vision is more sensitive to high frequency information such as edges, and (2) the number of effective coefficients in the synthetic blocks from the low frequency blocks is less than that from the high frequency blocks. Note that the variation of low frequency coefficients is larger. Whether the synthetic coefficients are from the high frequency blocks or the low frequency blocks is not an issue. Most importantly, the synthetic blocks and the input index vectors have same QDCT coefficients and the compatibility between different source blocks have been optimized.

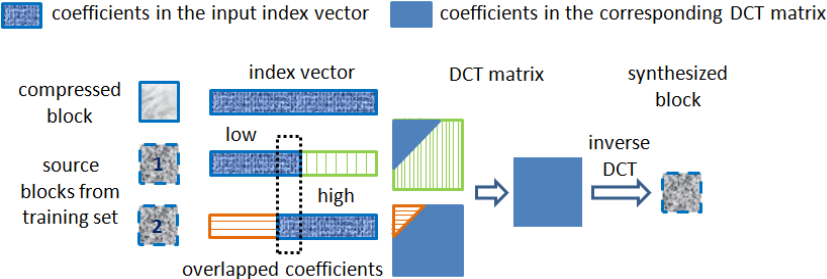


Fig. 14 Illustration of the block synthesis algorithm.

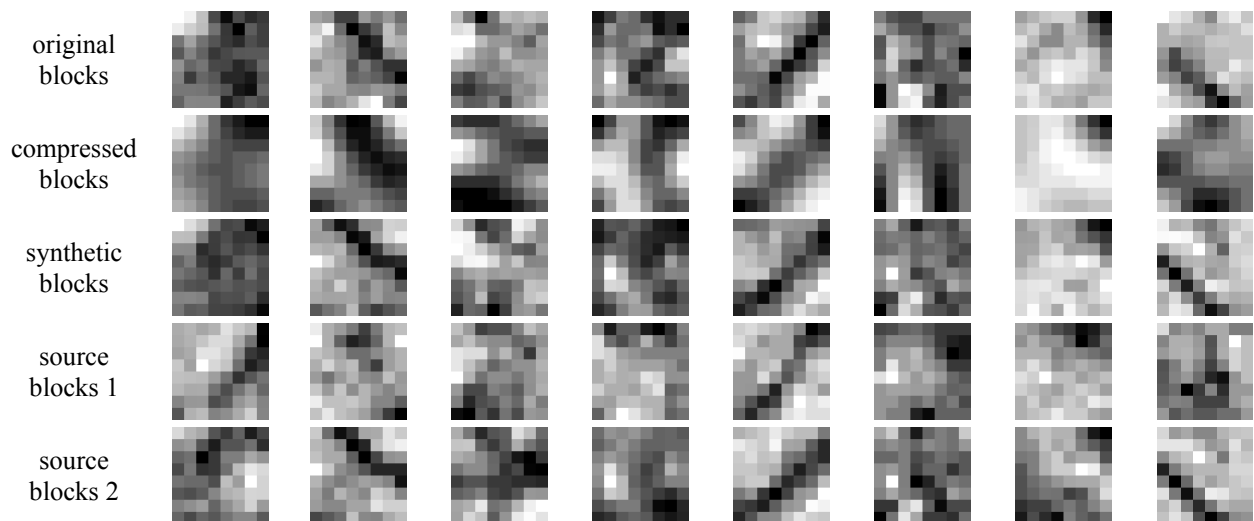


Fig. 15 Illustration of the block synthesis results. In the first row are original blocks of Y component. In the second row are the corresponding compressed blocks with the compression ratio of 86.92 and quality factor of 50. In the third row are the synthetic blocks. In the fourth and fifth rows are source blocks from the training set.

3.4. An Indexing Mechanism to Speed up the Algorithms

To make inference based on prior knowledge, a large training set is essential. Our training set contained more than 5 million block-pairs. It would be extremely time-consuming (about 20 hours) to search the entire training set exhaustively for each testing block. To speed up the searching, we propose an indexing mechanism using a multi-dimensional structure to store the information of each original block in the training set. The number of dimensions corresponds to the length of index vectors. Each entry represents one index vector and stores the information of the corresponding original blocks. This includes their positions in the source images and their hybrid neighborhoods. For a testing block, its index vector immediately leads us to the corresponding entry in the structure. This mechanism is faster than matching it with all the blocks in the training set.

This indexing mechanism cannot be used directly in the Y component, because its quantization steps are much smaller than those in U and V components. As a result, the number of different index vectors is too large to be stored in a multi-dimensional structure due to memory constraints. We preprocess the Y components of the original images by normalizing their intensity values to zero mean and unit variance.

Then we recalculate their index vectors whose varying range decreases significantly. This normalization step clusters the index vectors in Y components into a limited number of groups allowing storage in a multi-dimensional structure. In each entry of the subsequent structure, the un-normalized index vectors are added as extra information to distinguish individual blocks. This indexing mechanism makes it possible to handle such a large training set quickly and efficiently. The one-pass algorithm with the indexing mechanism were implemented using MATLAB on a PC embedded with an Intel® Core™2 Quad processor (3.0 GHz). Only one core was used in our implementation. Removing blocking artifacts in the Y, U and V components of a 448×512 image, it uses respectively 20, 5 and 5 minutes. Generally speaking, computational speed is not vital for forensic analysis. In the mentioned legal case, Kong and Craft had several weeks to process the evidence images.

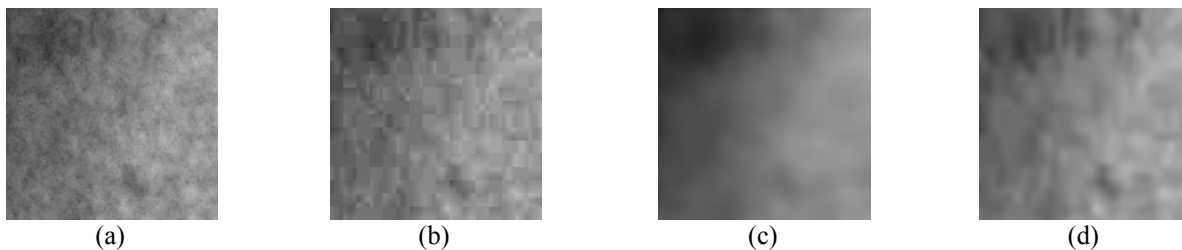
4. Experimental Results

To evaluate the KB approach, we performed extensive experiments and compared it with four other popular deblocking methods. The other methods were Sun et al.'s maximum a posteriori method based on a Field of Experts prior (FOE) which achieves higher PSNR gain [23], Foi et al.'s Pointwise Shape-adaptive DCT method (SADCT) which is one of the latest deblocking techniques [24], Luo et al.'s adaptive processing method (ADPROC) which is efficient at reducing blocking artifacts in smooth regions [25], and Chou et al.'s nonlinear filtering method (NLF) which is fast and robust for different images and quantization strategies [26]. These methods and the KB approach were analyzed using the two testing sets. The first testing set with 500 images was compressed with the JPEG quality factor of 50, and the average compression ratio was 72.55. The second testing set with 262 images was compressed with the JPEG quality factor of 25, and the average compression ratio was 126.93. As a result of this high compression ratio in the second set, most skin features were destroyed. As was mentioned in Section 3.2, the one-pass algorithm has similar performance to the Markov-model-based algorithm, but is much faster. Thus, the one-pass algorithm was used for the following evaluations. The U and V components were down-sampled

before deblocking, and their results were up-sampled and combined with the deblocked Y component. The same training set from the Asian database was used to generate all the experimental results.

In Figs. 16-21, we compare the original images (a), the compressed images (b), the results from FOE (c) [23], SADCT (d) [24], ADPROC (e) [25], and NLF (f) [26] methods. Additionally, the results from the KB approach (g) are shown. These six sets of skin images are shown for visual comparison. Figs. 16-18 are respectively Y, U and V components, and Figs. 19-21 are color images. The red circles in Figs. 19-21 denote skin marks identified by dermatology experts in the uncompressed images. The compression ratios of Figs. 16-21 are respectively 76.12, 69.50, 50.84, 115.32, 126.97, and 121.16. These figures show that FOE and SADCT methods have strong smoothing effect, which occasionally result in unrecognizable or absent vein patterns and skin marks; ADPROC and NLF methods have less smoothing effect, but they do not change the compressed images significantly; the KB approach removes the blocking artifacts and successfully recovers lost skin information, including the vein patterns and pigmented skin marks. Although in this paper, we emphasize blocking artifacts, the proposed KB approach is also capable of removing ringing artifacts because it is, in fact, a restoration algorithm.

To quantify these visual comparisons, we can either use image quality indices or carry out a subjective evaluation. It is well-known that the traditional point-wise comparison measures such as mean square error (MSE) or peak signal-to-noise ratio (PSNR) are not very well matched to perceived visual quality [27]. Other image quality indices, such as SSIM [28] attempt to mimic the extremely complicated human vision system (HSV). It is very difficult, if not impossible, to perfectly model HSV [29]. To avoid modeling defects, we carried out one subjective evaluation and three objective evaluations on the resultant images.



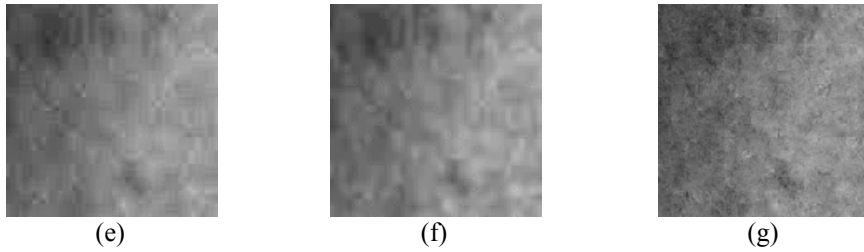


Fig. 16 Evaluation of deblocking performance in the Y component. (a) The Y component of an original skin image. (b) A compressed version of (a) with the compression ratio of 76.12 and quality factor of 50. (c)-(f) are the results from FOE [23], SADCT [24], ADPROC [25], and NLF [26] methods respectively. (g) The result from the KB approach.

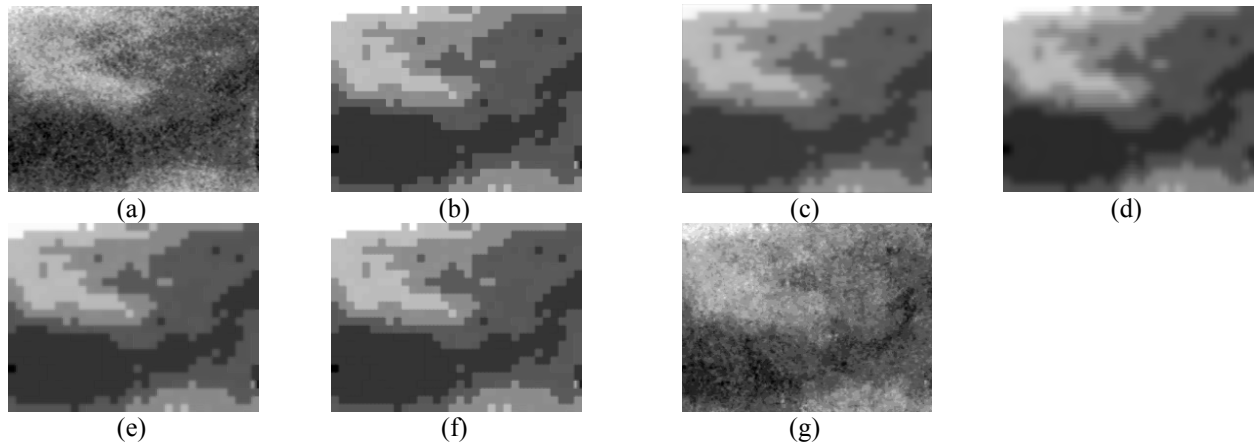


Fig. 17 Evaluation of deblocking performance in the U component. (a) The U component of an original skin image. (b) A compressed version of (a) with the compression ratio of 69.50 and quality factor of 50. (c)-(f) are the results from FOE [23], SADCT [24], ADPROC [25], and NLF [26] methods respectively. (g) The result from the KB approach.

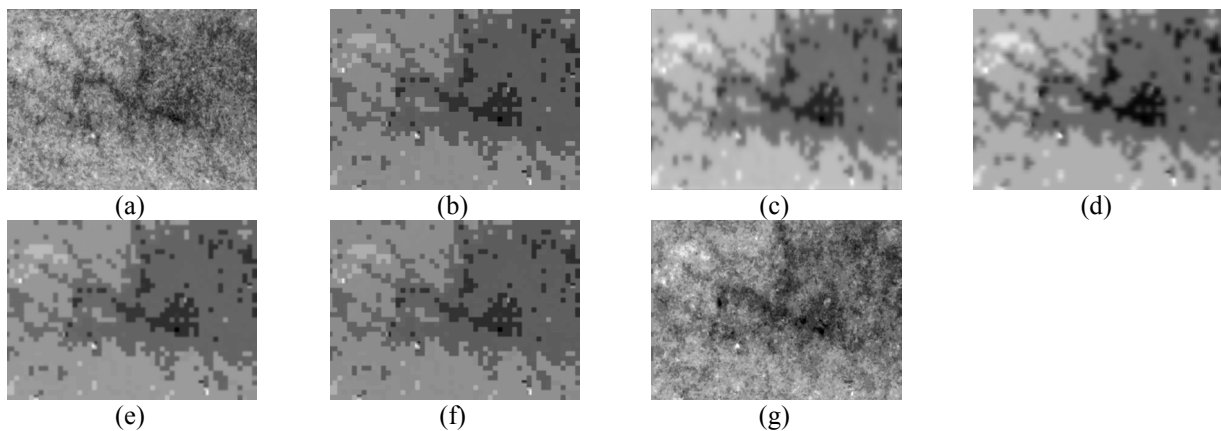


Fig. 18 Evaluation of deblocking performance in the V component. (a) The V component of an original skin image. (b) A compressed version of (a) with the compression ratio of 81.61 and quality factor of 50. (c)-(f) are the results from FOE [23], SADCT [24], ADPROC [25], and NLF [26] methods respectively. (g) The result from the KB approach.

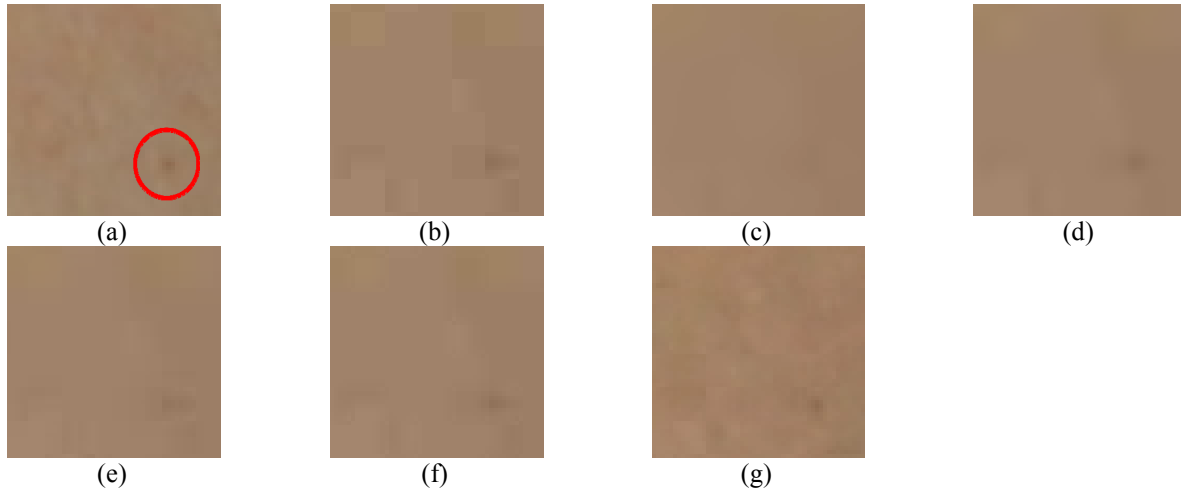


Fig. 19 Evaluation of deblocking performance in color images (example 1). (a) An original skin sub-image. The red circle denotes a pigmented skin mark identified by dermatology experts in the uncompressed image. (b) A compressed version of (a) with the compression ratio of 115.32 and quality factor of 25. (c)-(f) are the results from FOE [23], SADCT [24], ADPROC [25], and NLF [26] methods respectively. (g) The result from the KB approach.

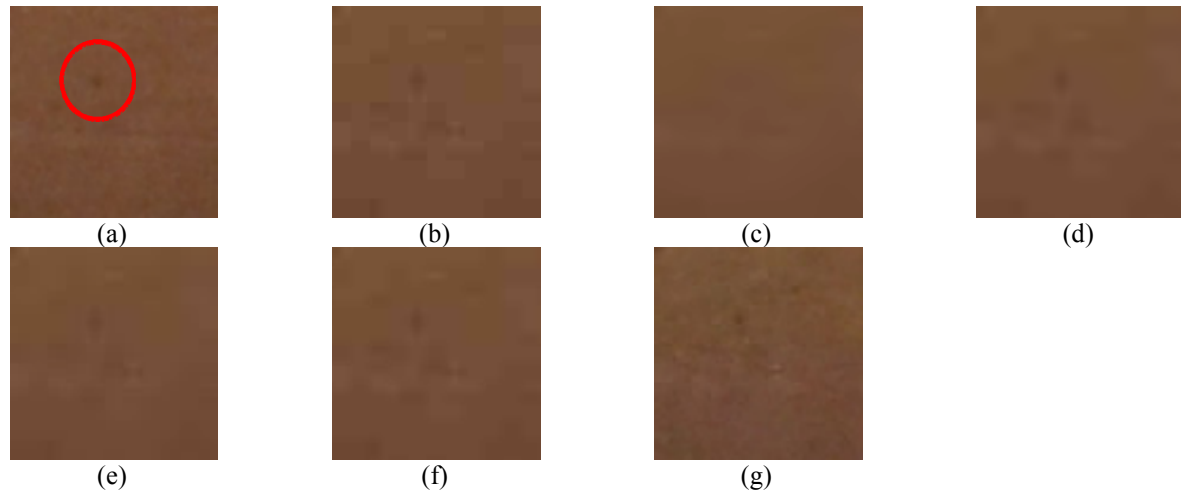


Fig. 20 Evaluation of deblocking performance in color images (example 2). (a) An original skin sub-image. The red circle denotes a pigmented skin mark identified by dermatology experts in the uncompressed image. (b) A compressed version of (a) with the compression ratio of 126.97 and quality factor of 25. (c)-(f) are the results from FOE [23], SADCT [24], ADPROC [25], and NLF [26] methods respectively. (g) The result from the KB approach.



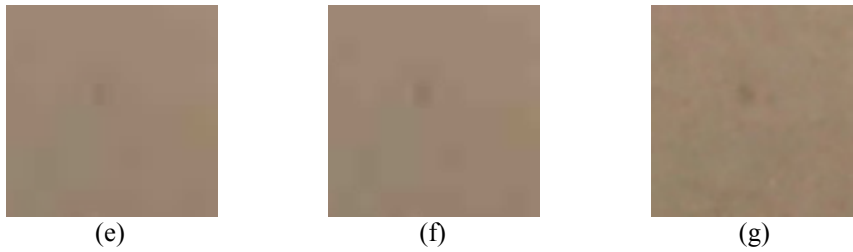


Fig. 21 Evaluation of deblocking performance in color images (example 3). (a) An original skin sub-image. The red circle denotes a pigmented skin mark identified by dermatology experts in the uncompressed image. (b) A compressed version of (a) with the compression ratio of 121.16 and quality factor of 25. (c)-(f) are the results from FOE [23], SADCT [24], ADPROC [25], and NLF [26] methods respectively. (g) The result from the KB approach.

4.1. Subjective Evaluation

Twenty-three observers participated in this experiment. Three of them had dermatological knowledge (one was a board-certified dermatologist and the other two were medical students studying dermatology); twelve of them were familiar with image processing; and the rest of them had computer science background. All the testing images were prepared by one person. It should be emphasized that there are no so-called skin mark examiners, like fingerprint examiners. Law enforcement agents, including the U.S. Department of Justice, recruit board-certified dermatologists to recognize skin marks in legal cases. The experiment was carried out in Y, U, V components and color images. In each case, 25 groups of images were presented. For Y, U and V components, 20 groups were from the first testing set, and 5 groups were from the second testing set, while for color images, 5 groups were from the first testing set, and 20 groups were from the second testing set. Totally 100 groups were evaluated. In each group, we presented an original uncompressed image (as reference), the corresponding compressed image, and the 5 resultant images (4 from the other methods and 1 from the KB approach) to the unbiased observers. We asked the observers to rate the images using a 10-point scale. For the Y, U and V components, the observers were required to rate the resultant images according to their similarity with the references. Higher grades (i.e., 10) represent more similarity between original uncompressed images and resultant images. For color images, skin marks in reference images were highlighted. An example is given in Fig. 19. Observers were asked to compare skin marks. As with the Y, U and V components, the same grading scheme was employed. Ten observers participated in the Y, U and V evaluation, and the other ten participated in the

color evaluation. The three dermatological professionals participated in all evaluations. The average scores from the dermatological professionals and from other participants are illustrated in Fig. 22 and Fig. 23, respectively. They show clearly that the KB approach provides the greatest visual quality improvement. These results pinpoint clearly that the KB approach is effective not only for generic skin images, but also for skin marks. They further confirm our visual comparison in Figs. 16-21.

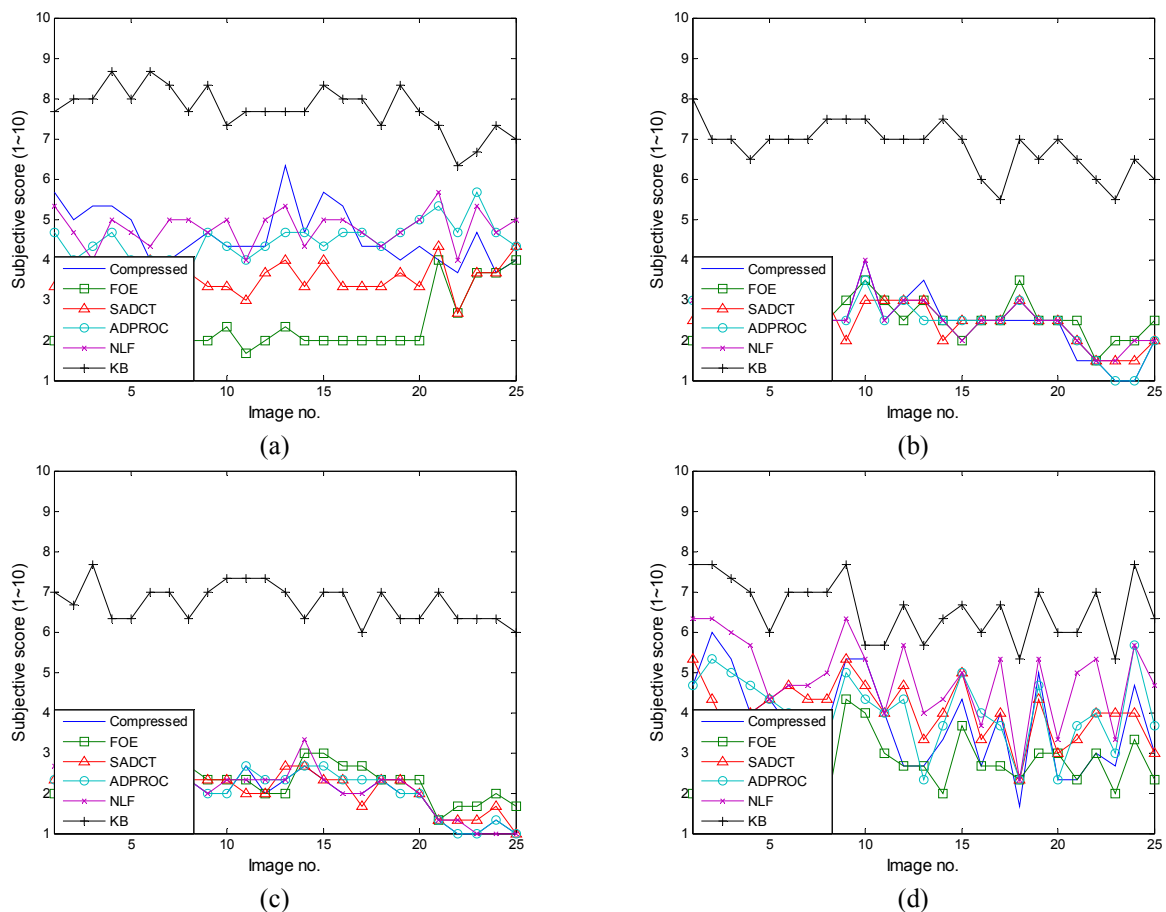


Fig. 22 Illustration of subjective evaluation results from the three dermatological professionals. Higher scores represent more similarity to the original image. (a) Y component, (b) U component, (c) V component, (d) color image.

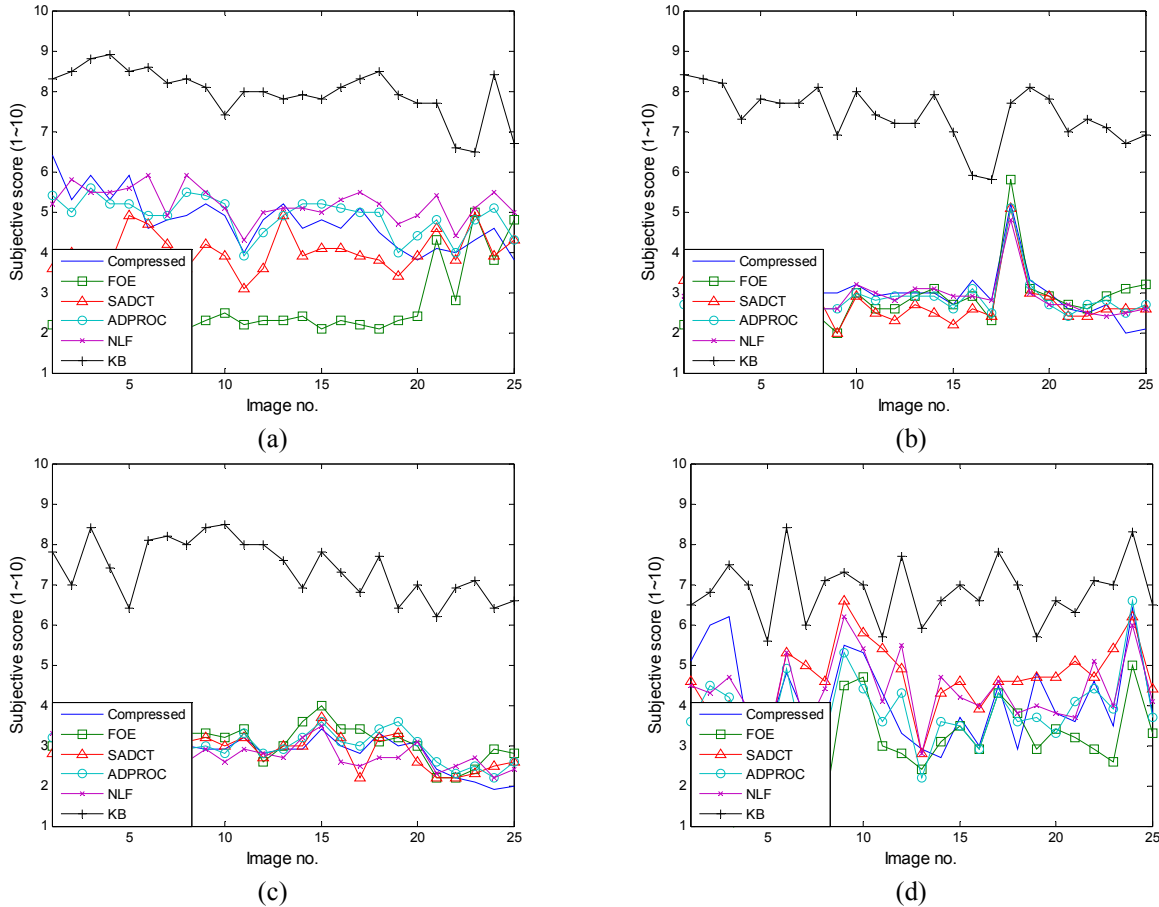


Fig. 23 Illustration of subjective evaluation results from the other participants. Higher scores represent more similarity to the original image. (a) Y component, (b) U component, (c) V component, (d) color image.

The application of the KB approach could improve confidence in diagnosis from digital images in real cases. The KB approach could reduce unnecessary debates in real cases because it significantly improves the visual quality of skin marks and other features for identification. The visual quality of images is important for accurate identification. Dermatology training is mostly based on “in person” physical exams and even enhanced visualization with dermatoscopes. Thus, digital diagnostic training is best performed when using uncompressed images. Although there is no absolute threshold for useable resolution, previous research demonstrates that image resolution is most important when trying to accurately identify small pigmented lesions such as those used in the test cases here [35].

4.2. Objective Evaluation based on Phase Information

In the previous experiment, we evaluated the KB approach in terms of the visual quality. In this experiment, we used phase information to obtain an objective evaluation. Phase is extremely important information for biometric recognition. The famous IrisCode is based on coarse representation of Gabor phases [30]. In addition to IrisCode, phases are also employed for palmprint and face recognition [31][32]. Behar et al. pinpoint that images can be reconstructed from localized phase [33]. Phase also has strong relationship with edges. Thus, we evaluated phases in the resultant images. To extract pure phase information in images I and J , where I is an original image, and J is a resultant image from one of the methods, we took the 2D Fourier Transform of I and J , and removed their magnitude information in the Fourier domain. Then, we took the inverse 2D Fourier Transform. Once we obtained the phases of I and J , the function

$$S(I, J) = \sum_{x=0}^{N-1} \sum_{y=0}^{M-1} \sum_{i=1}^B \sum_{j=1}^B |I_p(xB+i, yB+j)| \cdot |J_p(xB+i, yB+j)|, \quad (6)$$

where I_p (or J_p) is the phase of I (or J), B is a block size, and N and M are numbers of blocks in the column and row, respectively, is used to evaluate the similarity between the magnitude of the pure phase information in the two images. We divided the phase images into different blocks, because JPEG is a block-based algorithm. The block size varied from 8×8 pixels to 256×256 pixels. The higher value of S indicates more similarity between phases of I and J . We also evaluated the similarity of the entire image. The average measures for the Y, U and V components of the testing images are illustrated in Fig. 24. The standard deviations of the measures are illustrated in Fig. 25. The block synthesis algorithm was deployed for the Y component. The average percentage of synthetic blocks per image is 26.3% for the first testing set and 3.6% for the second testing set. In all settings, the results from the KB approach are clearly superior. In general, the similarity measures of the Y component were higher than those of the U and V components, due to the lower compression ratio in Y. In addition, for most of the results, the distributions of the results from the KB approach had the smallest standard deviations. This implies that the KB

approach performed more consistently on varying images. This objective evaluation demonstrates that the KB approach can successfully recover the phase information.

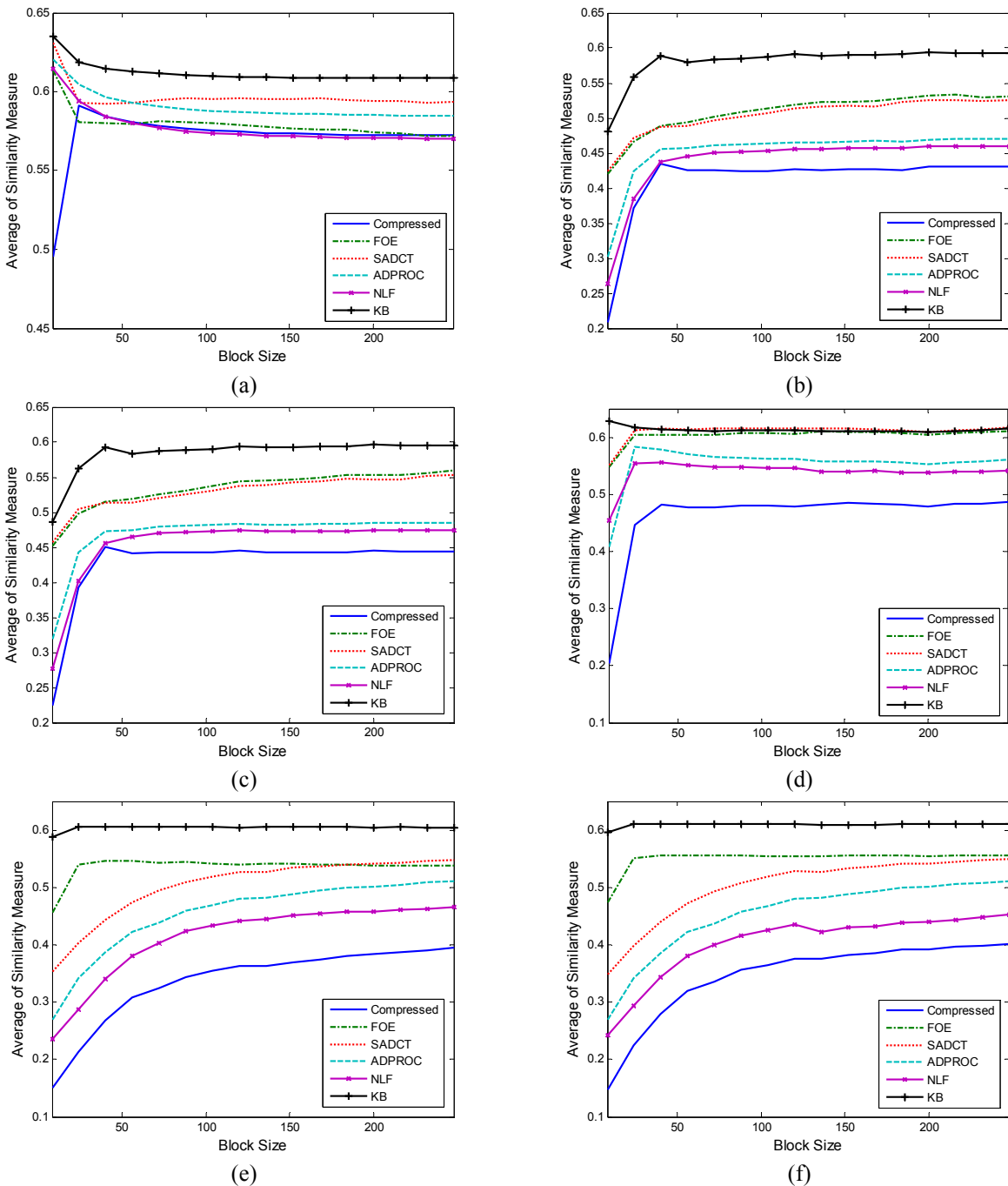
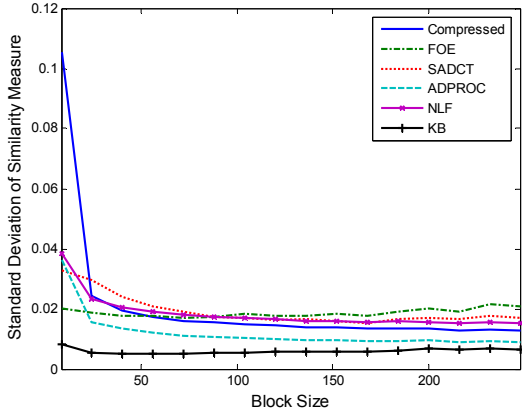
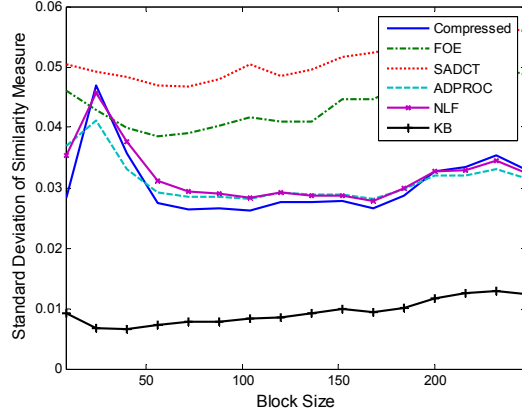


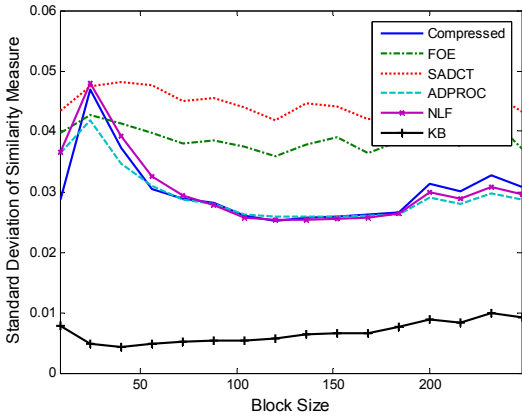
Fig. 24 Illustration of the average of similarity measures. (a), (b) and (c) are the results from the Y, U and V components of the 1st testing set; (d), (e) and (f) are the results from the Y, U and V components of the 2nd testing set.



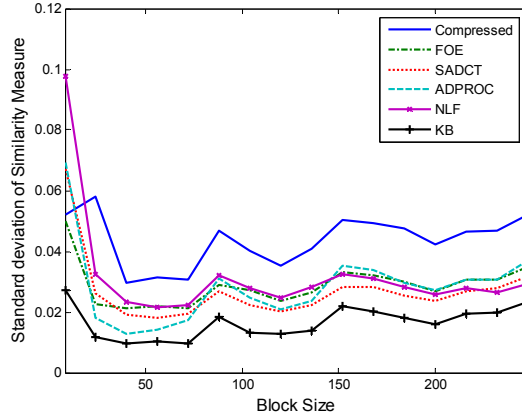
(a)



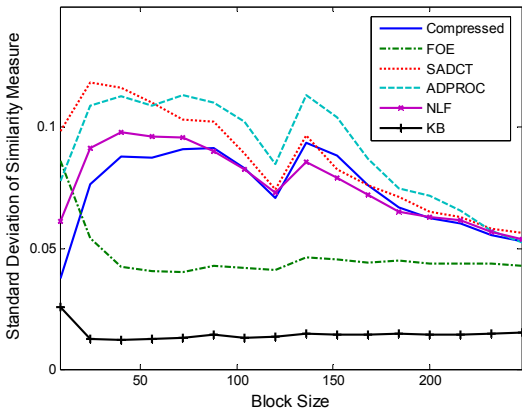
(b)



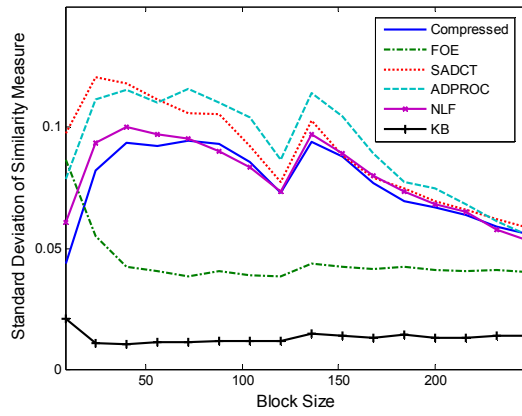
(c)



(d)



(e)



(f)

Fig. 25 Illustration of the standard deviation of similarity measures. (a), (b) and (c) are the results from the Y, U and V components of the 1st testing set; (d), (e) and (f) are the results from the Y, U and V components of the 2nd testing set.

4.3. Objective Evaluation based on Automatic Skin Mark Detection

In this subsection, an evaluation of recoverability of the proposed KB approach for skin marks is reported. Note that skin marks are important biometric traits for forensic analysis. For this evaluation, an automatic skin mark detection algorithm was designed. Given one training image (original image) and one testing image (original image or deblocked image) from the same body part of the same person, an image patch with a skin mark was cropped from the training image. The size of the image patch was 19×19 pixels. We used the 2D Fourier Transform to remove the magnitude information and used the pure phase information for detection. We also employed the same approach to remove the magnitude information in the testing image. The cosine measure was utilized to obtain the similarity between the skin mark patch from the training image and all possible 19×19 pixel image patches in the testing image. In an ideal case, the corresponding skin mark in the testing image should have the highest similarity. Because some of the testing images had more than one skin mark, if the corresponding skin mark in the testing image had the highest or the second highest similarity, it was regarded as a correct detection. For each deblocking algorithm, 150 image pairs (one is an original image and the other is a resultant image) from the Caucasian database were examined. The image size was 256×256 pixels. Table 1 lists the detection rates. It is clear that the proposed KB approach performed much better than other algorithms and its detection rate is close to that from matching two original images of the same person. These results indicate that the KB approach can effectively recover skin marks from compressed images to overcome quantization noise.

Table 1. Evaluation results of automatic skin mark detection rate

Original	Compressed	FOE [23]	SADCT [24]	ADPROC [25]	NLF [26]	KB
95.3%	49.3%	82.5%	80.2%	54.6%	62.1%	90.1%

4.4. Objective Evaluation based on a Blockiness Index

To evaluate discontinuity between blocks, we calculated the blockiness index [34] of the original, compressed, and resultant images. The range of this index is between zero and one. A higher value represents more serious discontinuity between blocks. The indices for the Y, U and V components of the two testing sets are listed in Table 2. Note that the block synthesis algorithm was used for the Y component. The KB approach is always the best compared with other methods and its resultant images are comparable to the original images.

Table 2. Evaluation results of the blockiness index

	The first testing set			The second testing set		
	Y	U	V	Y	U	V
Original	0.1311	0.1893	0.1472	0.2208	0.1898	0.1997
Compressed	0.3402	0.9565	0.9443	0.6861	0.9485	0.9584
FOE [23]	0.3607	0.5253	0.4315	0.4889	0.4190	0.4772
SADCT [24]	0.2274	0.5669	0.5078	0.4906	0.5100	0.6136
ADPROC [25]	0.2501	0.7353	0.6786	0.5932	0.7037	0.7748
NLF [26]	0.3092	0.6716	0.5983	0.3739	0.5957	0.8377
KB	0.1615	0.1914	0.1336	0.3676	0.1682	0.2380

5. Conclusion

In this paper, we have proposed a new knowledge-based approach to remove JPEG blocking artifacts in skin images for forensic analysis. This approach extracts prior knowledge of skin images from a training set, and uses it to infer original blocks in compressed evidence images. A Markov-model-based algorithm and a one-pass algorithm were developed to implement the inference. A block synthesis algorithm was designed to handle the cases where input compressed blocks are not contained in the training set. An indexing mechanism was employed to speed up these algorithms. The KB approach was evaluated on skin images from people with different races, genders and ages, taken under different imaging configurations, and with different compression ratios. Evaluations for visual quality, phase information, automatic skin mark detection and blockiness index demonstrated that the KB approach outperforms other deblocking methods. It successfully removes blocking artifacts and recovers lost skin mark information. Using the KB

approach, the visual quality of biometric features such as pigmented skin marks can be significantly improved.

Acknowledgements

We would like to thank the U.S. Department of Justice, Immigration and Customs Enforcement, Singapore Prison Service and the Singapore Police Force for their legal and forensic discussions. This work is partially supported by the Ministry of Education, Singapore through AcRF Tier 1.

Reference

- [1] U.S. Immigration and Customs Enforcement, “Ex-marine convicted of using drugs and force to have sex”, May, 29, 2008 (<http://www.ice.gov/pi/news/newsreleases/articles/080529losangeles.htm>)
- [2] Canada’s National Tipline for Reporting The Online Sexual Exploitation of Children, http://www.cybertip.ca/pdfs/fact_sheet_pdfs/English/CyberStats_en.pdf.
- [3] BBC, International Child Porn Ring Smashed 26 March 2001, <http://news.bbc.co.uk/1/hi/world/americas/1244457.stm>.
- [4] M. Motivans and T. Kyckelhaln, “Federal prosecution of child sex exploitation offenders, 2006”, Bureau of Justice Statistics, December, 2007 (<http://bjs.ojp.usdoj.gov/content/pub/pdf/fpcseo06.pdf>).
- [5] M.Y. Shen and C.C. Kuo, “Review of postprocessing techniques for compression artifact removal”, *Journal of Visual Communication and Image Representation*, vol.9, no.1, pp.2-14, 1998.
- [6] T.D. Tran, J. Liang, and C. Tu, “Lapped transform via time-domain pre- and post-filtering”, *IEEE TSP*, vol.51, no.6, pp.1557-1571, 2003.
- [7] J. Liang, C. Tu, and T.D. Tran, “Optimal block boundary pre/postfiltering for wavelet-based image and video compression”, *IEEE TIP*, vol.14, no.12, pp.2151-2158, 2005.
- [8] B. Macq, “Weighted optimum bit allocation to orthogonal transforms for picture coding”, *IEEE Journal on Selected Areas in Communications*, vol.10, no.5, pp.875-883, 1992.
- [9] K. Yamatani and N. Saito, “Improvement of DCT-based compression algorithms using poisson's equation”, *IEEE TIP*, vol.15, no.12, pp.3672-3689, Sep. 2006.
- [10] A. Z. Averbuch, A. Schclar, and D. L. Donoho, “Deblocking of block-transform compressed images using weighted sums of symmetrically aligned pixels”, *IEEE TIP*, vol.14, no.2, pp.200-212, 2005.
- [11] G. Zhai, W. Zhang, X. Yang, W. Lin, and Y. Xu, “Efficient image deblocking based on postfiltering in shifted windows”, *IEEE TCSVT*, vol.18, no.1, pp.122-126, 2008.
- [12] T. Chen, H. Wu, and B. Qiu, “Adaptive postfiltering of transform coefficients for the reduction of blocking artifacts”, *IEEE TCSVT*, vol.11, no.5, pp.594-602, 2001.
- [13] Y. Chang, and Y. Chen, “Design of a deblocking filter for both objective and subjective metrics”, *IEICE Transactions on Fundamentals of Electronics, Communications and Computer Sciences*, vol.E91-A, no.8, pp.2038-2040, 2008.
- [14] D. T. Vo, T. Q. Nguyen, S. Yea, and A. Vetro, “Adaptive fuzzy filtering for artifact reduction in compressed images and videos”, *IEEE TIP*, vol.18, no.6, pp.1166-1178, 2009.
- [15] K. Kwon, M. Yang, J. Ma, S. Im, and D. Lim, “Application of feedforward neural network for the deblocking of low bit rate coded images”, in *Proceedings of the 13th ICAIS*, pp.547-555, 2004.
- [16] G. Lakhani, “Image fitting using arctan for JPEG AC coefficient prediction”, *IEEE TCSVT*, vol.18, no.6, pp.791-802, 2008.
- [17] S.W. Hong, Y.H. Chan, and W.C. Siu, “A practical real-time postprocessing technique for blocking effect elimination”, in *Proceedings of the IEEE ICIP*, pp.21-24, 1996.

- [18] C. Weerasinghe, A. W. Liew, and H. Yan, "Artifact reduction in compressed images based on region homogeneity constraints using the projection onto convex sets algorithm", *IEEE TCSVT*, vol.12, no.10, pp.891-897, 2002.
- [19] J. Park, D. Park, R. J. Marks, and M. A. El-Sharkawi, "Recovery of image blocks using the method of alternating projections", *IEEE TIP*, vol.14, no.4, pp.461-474, 2005.
- [20] L. Guo, O. C. Au, M. Ma, X. Fan, Peter H. W. Wong and Daniel P. Palomar, "Image deblocking using convex optimization", in *Proceedings of the 15th IEEE ICIP*, pp.3148-3151, 2008.
- [21] W. T. Freeman, T. R. Jones, and E. C. Pasztor, "Example-based super-resolution", *Computer Graphics*, vol.22, no.2, pp.56-65, 2002.
- [22] W. T. Freeman, E. C. Pasztor, and O. T. Carmichael, "Learning low-level vision", *IJCV*, vol.40, no.1, pp.25-47, 2000.
- [23] D. Sun and W. Chan, "Postprocessing of low bit-rate block DCT coded images based on a fields of experts prior", *IEEE TIP*, vol.16, no.11, pp.2743-2751, 2007.
- [24] A. Foi, V. Katkovnik, and K. Egiazarian, "Pointwise shape-adaptive DCT for high-quality denoising and deblocking of grayscale and color images", *IEEE TIP*, vol.16, no.5, pp.1395-1411, 2007.
- [25] Y. Luo and R. K. Ward, "Removing the blocking artifacts of block-based DCT compressed images", *IEEE TIP*, vol.12, no.7, pp.838-842, 2003.
- [26] J. Chou, M. Crouse, and K. Ramchandran, "A simple algorithm for removing blocking artifacts in block-transform coded images". in *Proceedings of the IEEE ICIP*, vol.1, pp.377-380, 1998.
- [27] Z. Wang and A. C. Bovik, "Mean squared error: Love it or leave it? A new look at signal fidelity measures", *IEEE Signal Processing Magazine*, vol.26, no.1, pp.98-117, 2009.
- [28] Z. Wang, A. C. Bovik, H. R. Sheikh and E. P. Simoncelli, "Image quality assessment: from error visibility to structural similarity", *IEEE TIP*, vol.13, no.4, pp.600-612, 2004.
- [29] Z. Wang, A. C. Bovik and L. Lu, "Why is image quality assessment so difficult?", in *Proceedings of the IEEE ICASSP*, May 2002.
- [30] J. G. Daugman, "High confidence visual recognition of persons by a test of statistical independence", *IEEE TPAMI*, vol.15, no.11, pp.1148-1161, 1993.
- [31] D. Zhang, W.K. Kong, J. You and M. Wong, "On-line palmprint identification", *IEEE TPAMI*, vol.25, no.9, pp.1041-1050, 2003.
- [32] M. Savvides, B.V.K.V. Kumar and P.K. Khosla, "Eigenphases vs eigenface", in *Proceedings of the 17th ICPR*, vol.3, pp.810-813, 2004.
- [33] J. Behar, M. Porat and Y.Y. Zeevi, "Image reconstruction from localized phase", *IEEE TSP*, vol.40, no.4, pp.736-743, 1992.
- [34] C. Perra, F. Massidda and D.D. Giusto, "Image blockiness evaluation based on Sobel operator", in *Proceedings of the 12th IEEE ICIP*, pp.1-389-392, 2005.
- [35] D. A. Vidmar, D. Cruess, P. Hsieh, Q. Dolecek, H. Pak, M. Gwynn, K. Maggio, A. Montemorano, J. Powers, D. Richards, L. Sperling, H. Wong, and J. Yeager, "The Effect of Decreasing Digital Image Resolution on Teledermatology Diagnosis", *Telemedicine Journal*, vol.5, no.4, pp.375-383, 1999.



Chaoying Tang (S'11) received her B.Eng. and M.Eng. degrees, both in Automation, from Nanjing University of Aeronautics and Astronautics, China. She is now pursuing the Ph.D. degree at the School of Computer Engineering, Nanyang Technological University, Singapore. Her research interests include image processing, pattern recognition and biometrics.



Adams Wai-Kin Kong (M'03) received his PhD from the University of Waterloo, Canada. Currently, he is an assistant professor at the School of Computer Engineering, Nanyang Technological University, Singapore. His previous research includes algorithm design and analysis, system implementation and evaluation, feature analysis and template protection. Based on his palmprint identification algorithms, he was selected as a finalist of the 4th Young Inventor Awards 2002-2003, organized by Hewlett Packard and Fair Eastern Economic Review. In the summer 2008, he served as an expert witness to the US Department of Justice for a case of child sexual abuse. His papers have

been published in TPAMI, TIP, TIFS, TSMC, TCSVT, CVPR and pattern recognition. He has developed five patents; four of his patents have been approved, and the other has been filed. His research interests include biometrics, forensics, image processing, and pattern recognition.



Noah Craft received his M.D. and Ph.D. from UCLA School of Medicine and UCLA Molecular Biology Institute, respectively. He performed his post-doctoral research in the laboratory of Jeffery F. Miller working on melanoma and leishmaniasis immunology. His clinical interests include tropical dermatology and the development of online visual medicine diagnostic decision support (www.visualdx.com) and training tools (learnderm.org) for professionals and for patients (skinsight.com). Dr. Craft is based at Los Angeles Biomedical Research Institute at Harbor-UCLA Medical Center. He is the course chair for general dermatology at Harbor-UCLA, the director of teledermatology for UCLA, and the associate program director for the Harbor-UCLA dermatology residency program. He has published over 40 peer-reviewed manuscripts, 17 book chapters, and is the senior editor of a popular dermatology textbook. He has received over 25 NIH sponsored and other research grants to support his basic science, translational, and clinical trials research.